River Flow 2010 - Dittrich, Koll, Aberle & Geisenhainer (eds) - © 2010 Bundesanstalt für Wasserbau ISBN 978-3-939230-00-7

Scalar dispersion in strongly curved open-channel flows

W. van Balen
HKV Consultants, Lelystad, The Netherlands; formerly Faculty of Civil Engineering and Geosciences, Delft University of Technology, Delft, The Netherlands

Wim S.J. Uijttewaal
Faculty of Civil Engineering and Geosciences, Delft University of Technology, Delft, The Netherlands

K. Blanckaert
ICARE-ENAC, Ecole Polytechnique Fédérale, Lausanne, Switzerland and Faculty of Civil Engineering and Geosciences, Delft University of Technology, Delft, The Netherlands

ABSTRACT: Large-eddy simulations (LES) and Reynolds-averaged numerical simulations (RANS) are performed for the flow and scalar dispersion through a strongly curved open-channel bend. The aim of the study is to investigate the performance of both LES and RANS as regards the reproduction of the key bend flow features and the associated prediction of scalar spreading along the flume. In this respect, three different issues are addressed. Firstly, the influence of the water depth on the flow behavior as computed by LES and RANS is considered. Secondly, the plume statistics of the case with a continuous vertical line source is investigated. And thirdly, the dispersion behavior of a scalar tracer is studied by means of the case in which a blob of the scalar tracer is instantaneously injected. It is found that the LES computations fairly well reproduce the main flow features, whereas RANS computations experience severe difficulties in predicting the flow field. Moreover, it was found that the gradient-hypothesis of diffusion is only limitedly valid; even counter-gradient diffusion is observed. In addition, the residence time characteristics of the instantaneously injected blob of the scalar tracer in the bend are addressed as well.

Keywords: Large-eddy simulation, Scalar spreading, Curved open-channel flows.

1 INTRODUCTION

An important issue for present day environmental fluid mechanics and river engineering is the adequate prediction of scalar spreading through natural streams, such as the flow through urban areas, coastal areas and rivers. For instance in the case of river flows, water quality engineers have to cope with several relevant aspects such as ecological aspects, drinking water purposes and so forth. For these purposes, one should be able to properly predict the spreading of pollutants, for instance discharging cooling water by surrounding factories, properly. But also the spreading and mixing of nutrients, oxygen and heat is relevant from an ecological point of view for instance within the context of injection points for waste water outfalls.

Scalar dispersion in open-channels is studied extensively by many researchers. In this context the sizeable work of Fisher (1969) as well as the work of, among others, Demuren & Rodi (1986), Deng *et al.* (2001) and Shiono & Feng (2003) can be mentioned. However, although some attention is paid to the analysis of scalar spreading through straight open-channels by means of Large-Eddy Simulation (LES) (cf. Wang *et al.* (2005), no attention is paid to the scalar spreading prediction through curved open-channel by means of LES.

The aim of this paper to fill this gap by computing the scalar spreading through the strongly curved open-channel flow, as investigated by Blanckaert (2009). Moreover, the gained results will be used to comment on the validity of the gradient-diffusion hypothesis for the turbulence scalar fluxes and the dependency of the scalar transport on the water depth. The outline is as follows. In section 3, the main flow features are brieflyaddressed . In section 4 and 5, the results of simulations of the spreading from a certain source are given. First, the numerical model is described.

2 MODEL SETUP

2.1 *The numerical model*

The used LES model resolves the full three-dimensional Navier-Stokes equations, spatially filtered by a top-hat filter defined by the grid

spacing. The subgrid-scale stresses, arising from the filtering operation, are modeled using the standard Smagorinsky model with an associated model constant of 0.1, which is reduced near solid walls with a standard Van Driest damping function. RANS type simulations have been performed using the standard linear k-epsilon model.

The equations are discretized on a staggered mesh using finite volumes, where all the fluxes are approximated with central differences. The grid is Cartesian in straight parts of the geometry and cylindrical in curved parts. A second order explicit Adams-Bashforth method is used for advancement in time. The pressure Poisson equation is solved by cosine transformations in the cross-section and Gaussian elimination in streamwise direction.

In order to adequately deal with steep gradients in the concentration field, flux limiters are implemented to avoid spurious oscillations due to the discretization of the advection terms. For that purpose, the Van Albada flux limiter is incorporated in the advection-diffusion equation to be solved.

In our simulations of curved open-channel flow, the free surface is treated as a horizontal rigid lid where free-slip conditions are applied. Hydraulically smooth solid walls are represented by a wall-function that includes the viscous layer, the buffer layer and the logarithmic layer. Hydraulically rough walls are treated with an associated modified log-law.

2.2 *The computational setup*

The geometry and flow conditions of the experiment by Blanckaert (2009) are adopted (see figure 1). The discharge is 89 l/s. The bottom is hydraulically rough with a modeled roughness height of 6 mm, whereas the sidewalls are hydraulically smooth. In the numerical simulation, both the straight inflow and straight outflow have a length of 3.8 meters each (figure 1). The three investigated cases, denoted as the shallow, the medium and the deep case, are described in table 1. The flow is simulated using LES *and* RANS on a computational grid with 1260 x 192 x 24 cells in the longitudinal, lateral and vertical direction respectively. Both in the LES and RANS computations, the solid boundaries are treated with a standard wall-function, based on the logarithmic law-of-the-wall for either flow over a hydraulically smooth wall or a hydraulically rough wall.

Table 1. Hydraulic parameters of the three simulations. The three cases are henceforth denoted as the shallow case, the medium case and the deep case.

H [m]	R [m]	B [m]	Q [l/s]	V_{av} [m/s]	Re	Fr	R/H	B/H
0.108	1.7	1.3	60	0.43	46440	0.42	15.7	12.0
0.159	1.7	1.3	89	0.43	68400	0.34	10.7	8.2
0.206	1.7	1.3	115	0.43	88580	0.30	8.3	6.3

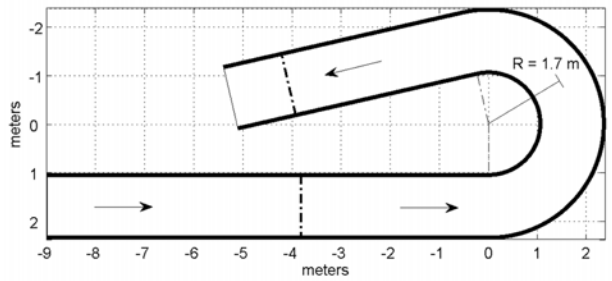

Figure 1. Flow geometry of the experimental setup investigated by Blanckaert (2002). The dashed lines denote the inflow and outflow boundary of the computational domain.

3 FLOW DESCRIPTION

In this section, a brief overview is offered of the main flow features observed in the experiments and numerical simulations of the strongly curved open-channel flow at three different water depths (also see Van Balen *et al*. (2010)).

The main curvature induced secondary flow cell, covering the entire width of the cross-section apart from the outer bank cell region, becomes stronger with increasing water depth as long as the flow is spatially developing. The computed strength by LES is in fair agreement with their experimental equivalents, whereas the RANS computations underestimated the center region cell strength, particularly at large water depths.

Van Balen *et al*. (2010) have shown that in the inner bank region an internal shear layer emerges due to the strong curvature of the flow. The curvature is not strong enough though to let the boundary layer detach from the convex inner bank. This internal shear layer gains influences and strength as the water depth increases and is properly simulated by LES, whereas the RANS (with standard k-epsilon closure model) fails to reproduce it.

At the outer bank, a secondary flow cell occurs with the opposite rotational sense compared to the dominant curvature induced helical motion. This outer bank cell strengthens with increasing water depth and is the strongest in the upstream part of the bend, both in the experimental results and in the LES results, although it disappears far downstream in the LES results. RANS, however, did not reproduce this outer bank cell.

4 SPREADING FROM A LINE SOURCE

The simulation runs described in table 1, are used for the present investigation of the spreading from a vertical line source. This vertical line source is located at the entrance of the bend for all the three cases.

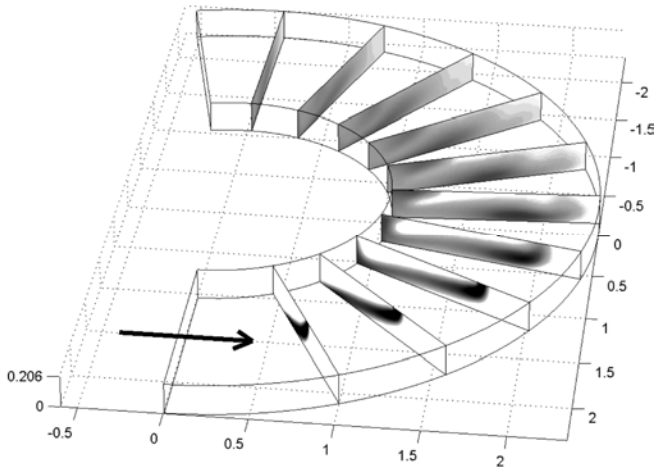

Figure 2. Time-averaged concentration distribution for the deep case as predicted by the LES computation. Distances are in meters. The arrow denotes the flow direction.

The line source is located half-way the width of the flume and is stretched over the entire water depth. The concentration c is considered as scaled with an arbitrarily chosen reference value C_0. At the line source, the concentration is fixed on $c/C_0 = 1$ as a constant boundary condition. The time-step of the simulation is taken constant dt = 2 ms, in order to keep the incoming concentration flux constant. In the following, the Reynolds decomposition of the velocities and the concentration is denoted similarly as $u = U + u'$ and $c = C + c'$ for the velocities and concentration respectively, in which the mean part is denoted with a capital and the fluctuating part is denoted with a prime.

The computational results for the time-averaged concentration field along the flume are shown in figure 2 for the LES computation and in figure 3 for the RANS computation, both for the deep case (H = 0.206 m). In figures 2 and 3, it is seen that the scalar is rather well mixed along the flume by the secondary flow.

In the previous section, we have identified the inner bank region, the outer bank region and the center region as the areas where the key features of flow occur. These features leave a clear footprint in the pattern of the concentration plume. The main feature is obviously the center region, where the classical helical motion effectuates a mixing of the solute in the cross-sectional plane. Since we know that the center region cell strength is much weaker in the RANS results, it is not surprising that the cross-sectional spreading of the solute is less effective in the RANS computation. This is clearly seen in the upstream part of the bend in figures 2 and 3.

Also as a result of this difference in center region cell strength, the concentrations near the inner bank are much higher in the LES result compared to the RANS result.

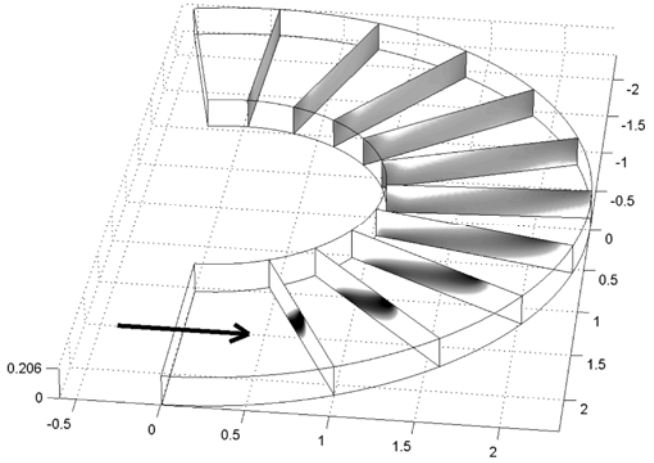

Figure 3. Time-averaged concentration distribution for the deep case as predicted by the RANS computation. Distances are in meters. The arrow denotes the flow direction.

The internal shear layer is analogously present for the deep case (H = 0.206 m) and is characterized by relatively low streamwise velocities and a reduced secondary flow strength. Figure 2 shows for this deep case (H = 0.206 m) that in the inner bank region accumulation of the solute occurs (beyond approximately 90°) due to this reduction of streamwise and transverse velocities, whereas this is not seen in the RANS result shown in figure 3.

The outer bank cell is absent in the RANS results, whereas it is present in the LES result, be it not along the entire flume length. This outer bank cell has a width that is approximately equal to the water depth. For the deep case, shown in figures 2 and 3, the outer bank cell is present in the LES result from the 0° cross-section up to approximately the 130° cross-section. Figure 3 shows that in the RANS computation the solute easily reaches the outer bank, whereas figure 2 shows that in the LES computation the outer bank region is a region with relatively low concentrations. Apparently, the concentration plume can hardly penetrate the outer bank cell due to its opposite sense of rotation compared to the center region cell. Also far downstream, as the outer bank cell has vanished in the LES result, the outer bank region is still a region with low concentrations.

In order to show the differences between the three cases with different water depth, the time-averaged contaminant concentration distribution is shown in figure 4 for the 90° cross-section. This cross-section is situated approximately halfway the bend. Recall that upstream of this cross-

section the center region cell strength has been the strongest for the deep case and the weakest for the shallow case. Figure 4 shows, in addition to figure 2, how the initially vertical line source is skewed by the flow. Particularly the shallow case reveals a diagonal ribbon across the cross-section.

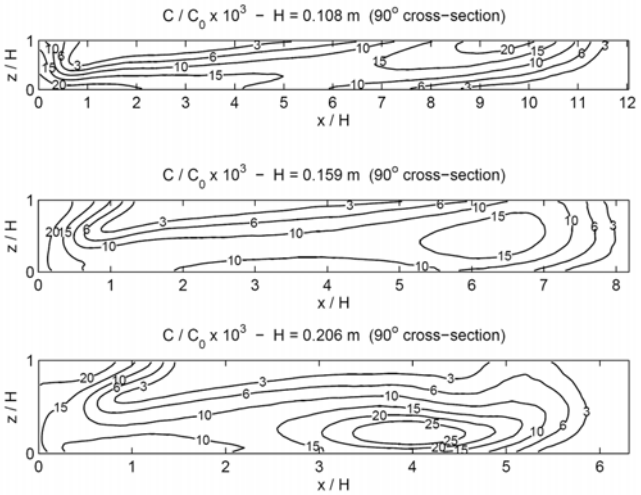

Figure 4. Time-averaged concentration distribution at the 90° cross-section as predicted by the large-eddy simulation. From top to bottom: the shallow case, the medium case and the deep case. From left to right denotes from inner bank to outer bank.

Moreover, figure 4 shows that the outer bank region contains little contaminant because of the difficulty that is experienced by the plume to penetrate the outer bank cell, which has a width that is approximately equal to the water depth. In figure 4, generally two local maxima are seen: one near the inner bank and one in the outer half of the cross-section. The locations of these maxima for the three cases reflect the differences in the center region cell strength for the three cases. Whereas for the shallow case these maxima are found at the bottom in the inner half of the cross-section and at the free surface at the outer half of the cross-section, the maxima for the deep case are found at the free surface in the inner half of the cross-section and near the bottom in the outer half of the cross-section. This indicates that the flow at the 90° cross-section in the deep case is further in its spiral cycle compared to the flow at the same location in the shallow case.

The 90° cross-section of the medium case (with H = 0.159 m) is used to highlight the statistics of the plume. The associated concentration distribution is shown in the middle panel of figure 4. The variables u, v and w denote the velocities in transverse, streamwise and vertical direction respectively. In the upper panel of figure 5, the root-mean-square fluctuations of the concentration is shown. In this panel, it is seen that the intensities of the concentration fluctuations in some parts of the cross-section are of the same order of magnitude as the concentration itself. The highest intensities of the concentration fluctuations are found (not shown here) in the vicinity of the line source, which is in accordance with the findings of Fackrell & Robins (1982) and Wagner *et al*. (2007). Furthermore, it was found that in the inner bank region, the intensities of the concentration fluctuations are low whereas the concentration itself is high. This indicates the existence of persistent moderate concentrations. In the outer bank region, the intensities of the concentration fluctuations are high whereas the concentration itself is low which is associated with intermittent occurrences of stronger concentration structures (cf. Crimaldi *et al.* (2002)).

The cross-sectional components of the Reynolds fluxes $\langle u'c' \rangle$ and $\langle w'c' \rangle$, shown in the second and fourth panel of figure 5, reveal the strong influence of the secondary flow as a positive and a negative layer emanate on top of each other. Such a two-layer structure was also found for the $\langle v'c' \rangle$ fluxes up to approximately the 70° cross-section. In the area of the bend further downstream, this two-layer structure is spoiled. This can be seen in third panel of figure 5. This destruction of the two-layer structure also occurs for the $\langle u'c' \rangle$ and $\langle w'c' \rangle$ stresses, be it further downstream in the bend. In the inner bank region of the cross-section, the internal shear layer leaves a pronounced footprint in the pattern of the $\langle v'c' \rangle$ fluxes.

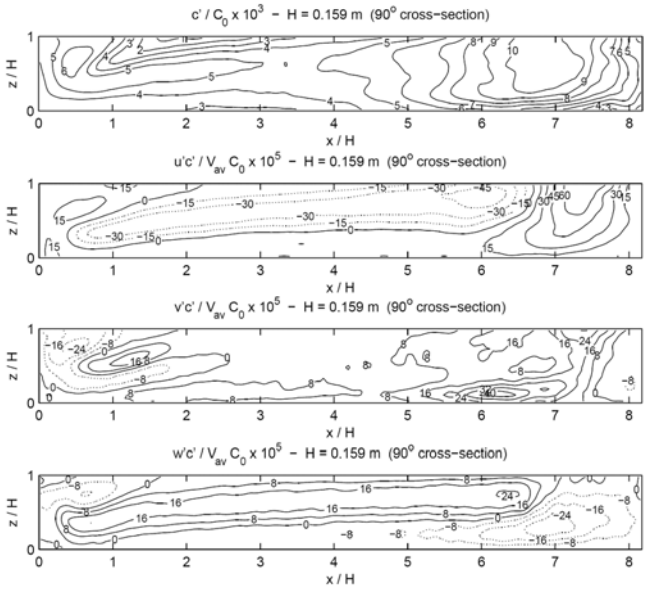

Figure 5. Plume statistics at the 90° cross-section as predicted by the large-eddy simulation. From top to bottom: the root-mean-square fluctuations of the contaminant concentration and the three Reynolds fluxes. From left to right denotes from inner bank to outer bank.

In order to model the spreading of pollutants, the gradient-diffusion hypothesis is widely used. In a cylindrical reference system, the relation be-

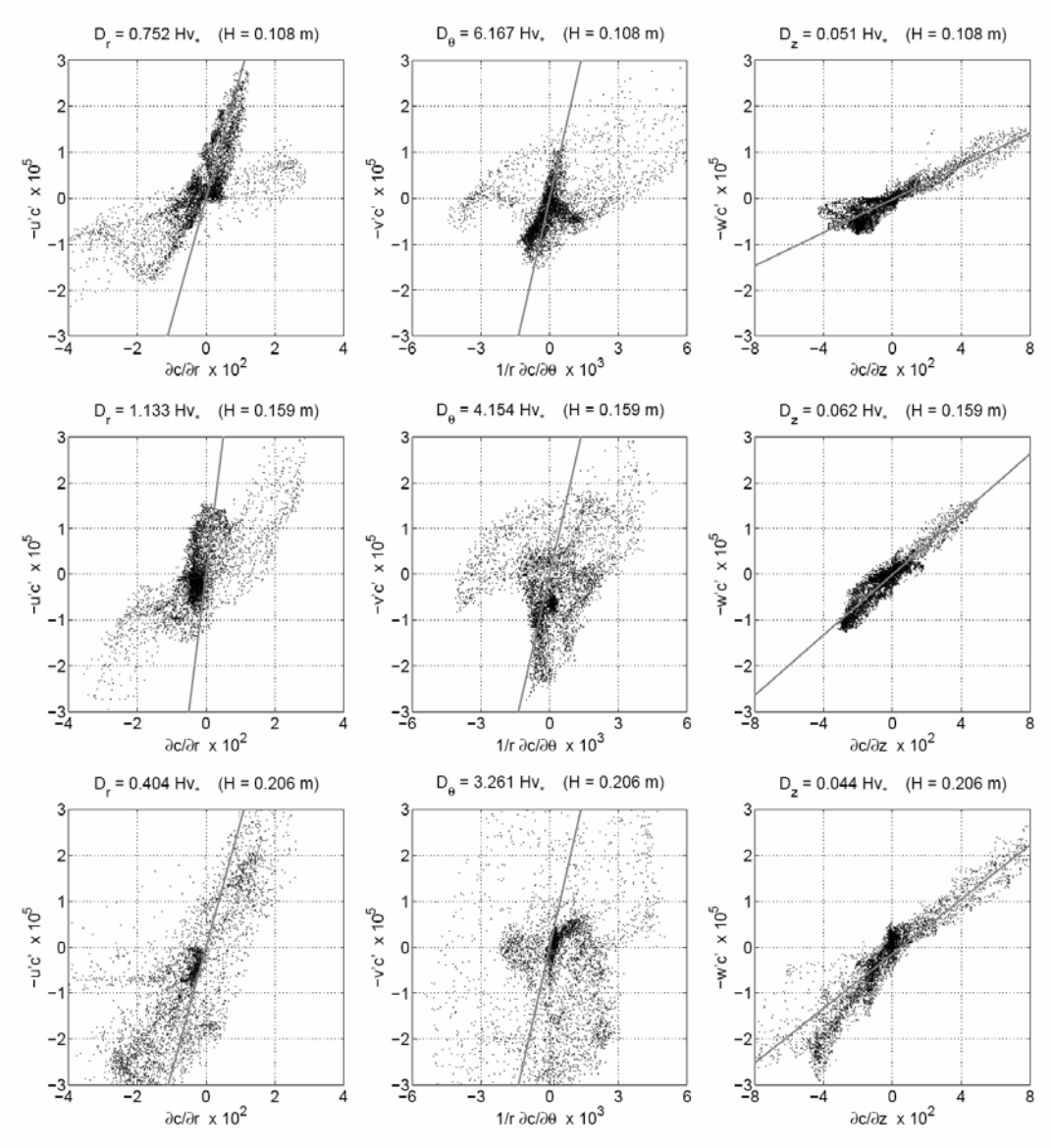

Figure 6. From top to bottom: the shallow, the medium and the deep case. From left to right: diffusion coefficients in transverse, streamwise and vertical direction. The coefficients (shown in the titles of the figures) are scaled with the water depth H and the friction velocity v*. The straight lines represent linear fits through the scattered data.

tween the Reynolds fluxes and the concentration gradients is given by

$$-\left\langle u'_i\, c'\right\rangle = D_i \frac{\partial C}{\partial x_i}, \qquad (1)$$

where D_i represents D_r, D_θ and D_z which are the eddy diffusion coefficients in transverse, streamwise and vertical direction respectively.

The present results are useful for investigating whether the gradient-diffusion hypothesis is actually valid and to what extent isotropy (i.e. $D_r = D_\theta = D_z$) can be assumed. To obtain the eddy diffusion coefficients, the values of the Reynolds fluxes are plotted against the associated concentration gradient. The diffusion coefficient is then captured as the slope of the linear fit through the scatter-plot (cf. Muppidi & Mahesh (2008)). For this purpose, the 180° cross-section is chosen since this is the location in the bend where the contaminant is most well mixed. The results of this approach are shown in figure 6. The values of the obtained diffusion coefficients are shown in the titles of the pictures, made non-dimensional with the water depth H and the friction velocity v_*.

Figure 6 shows that the linearly dependency of the Reynolds flux on the concentration gradient is basically only valid for the vertical direction. Particularly for the medium case (H = 0.159 m), a clear linear profile is found. The computed non-dimensional vertical diffusion coefficients vary from 0.044 to 0.062. A clear dependency of this value on the water depth cannot be seen. The linear dependency is much less clearly seen in the transverse direction; however, it seems to hold for a part of the results. The computed non-dimensional transverse diffusion coefficients vary from 0.40 to 1.13. The results for the streamwise

direction do not show any linear dependency at all, which gives the obtained non-dimensional streamwise diffusion coefficients, varying from 3.3 to 6.2, a highly speculative character.

The computed eddy diffusion coefficients, although having a speculative character in some directions, show that the isotropy assumption is far from valid, since the ratios between the coefficients in the several directions are of the order of 10. The streamwise diffusion coefficients is even 100 times larger than the vertical diffusion coefficient.

An implication of the gradient-diffusion hypothesis is that the direction of the Reynolds flux of the contaminant is aligned with the direction of the mean concentration gradient, since the diffusion coefficient is assumed to be a positive scalar. As a consequence, all the points in the scatter plot of figure 6 should be situated in the lower left quadrant and the upper right quadrant (cf. Muppidi & Mahesh (2008)). However, since this is not the case for the transverse transport and particularly the streamwise transport, one might speak of counter-gradient diffusion in some parts of the cross-section. This counter-gradient diffusion is also addressed by Muppidi & Mahesh (2008) in the results of their direct numerical simulation of skewed jet flow and is discussed in more detail by Tagawa *et al*. (2002) who have performed measurements in a curved rectangular duct.

5 SPREADING OF A SCALAR BLOB

In order to further exploit the strength of the simulation method, we instantaneously inject the contaminant over an area covering the entire width and the entire depth of the flow over a length of approximately half a meter. The initial situation is shown in the top left panel of figure 7. The concentration in this area is $c/C_0 = 1$. The other panels of figure 7 show how the injected blob disperses throughout the flume for the deep case at several stages in time, namely after 3 s, 6 s, 10 s, 15 s and 20 s. In these pictures, the instantaneous depth-averaged concentration is shown.

In figure 7, it can be seen in the situation that after 3 s that the flow and the contaminant first enter the bend near the inner bank, i.e. the area the highest velocities are found. The situation after 6 s clearly shows the three aforementioned important areas of the flow: the inner bank region (the area of the internal shear layer), the center region (the area of the classical helical motion) and the outer bank region (the area of the outer bank cell). These three areas are almost separate of each other as two filament-like bands of relatively low concentrations are seen in between the three areas.

The situation after 10 s shows that the contaminant in the inner bank region and the center region have pretty well mixed up, whereas the contaminant in the outer bank region still slowly moves forward. This indicates that the outer bank region more or less acts like a dead zone, where the contaminant can remain present for a relatively long time. Another interesting observation in the picture after 10 s is the presence of coherent structures at the rim of the concentration field near the outer bank. These coherent structures represent downwellings of fluid at the interface of the center region cell and the outer bank cell.

The figures showing the concentration field after 15 s and 20 s show how the contaminant leaves the flume. Again, in these two pictures it is clearly seen how slowly the contaminant near the outer bank is moving. After about 30 s the curved part of the flume is fully clean again.

The residence time of the contaminant in the curved part of the bend is investigated by means of integrating the concentrations only over the curved part of the domain and afterwards normalizing the obtained value by the total injected amount of mass.

In figure 8, it is shown for the three different cases how large the relative amount of mass in the curved part of the domain is during about 30 s after release. The time t is normalized using the bulk velocity V_{av} and the length of the curved part of the flume along the center line, denoted as L. The normalized time is denoted as $\langle t \rangle$. Figure 8 shows that only that part of the picture is interesting that represents the outflow of the contaminant out of the curved part of the domain to the straight outflow reach of the domain. The rate at which the contaminant leaves the curved part of the flume is defined as minus the time-derivative of the curves shown in left panel of figure 8. The results for the outflow rate are shown in right panel of figure 8. This process of outflow of the contaminant can roughly be divided into three stages: *A*. the period $0.7 < \langle t \rangle < 0.9$, *B*. the period $0.9 < \langle t \rangle < 1.2$ and *C*. the period $1.2 < \langle t \rangle < 1.9$.

The overall observation for the shallow case was that the contaminant very gently flows through the bend and leaves the bend since the flow in this case is hardly hindered by the decelerating effects of the internal shear layer or the outer bank cell. As shown in figure 7, these decelerating effects are present in the medium case and very strongly present in the deep case. These decelerating effects leave a footprint in figure 8 as follows.

During stage *A*., the contaminant can very effectively leave the bend in the shallow case because of the absence of the the internal shear layer near the inner bank: figure 7 shows that the con-

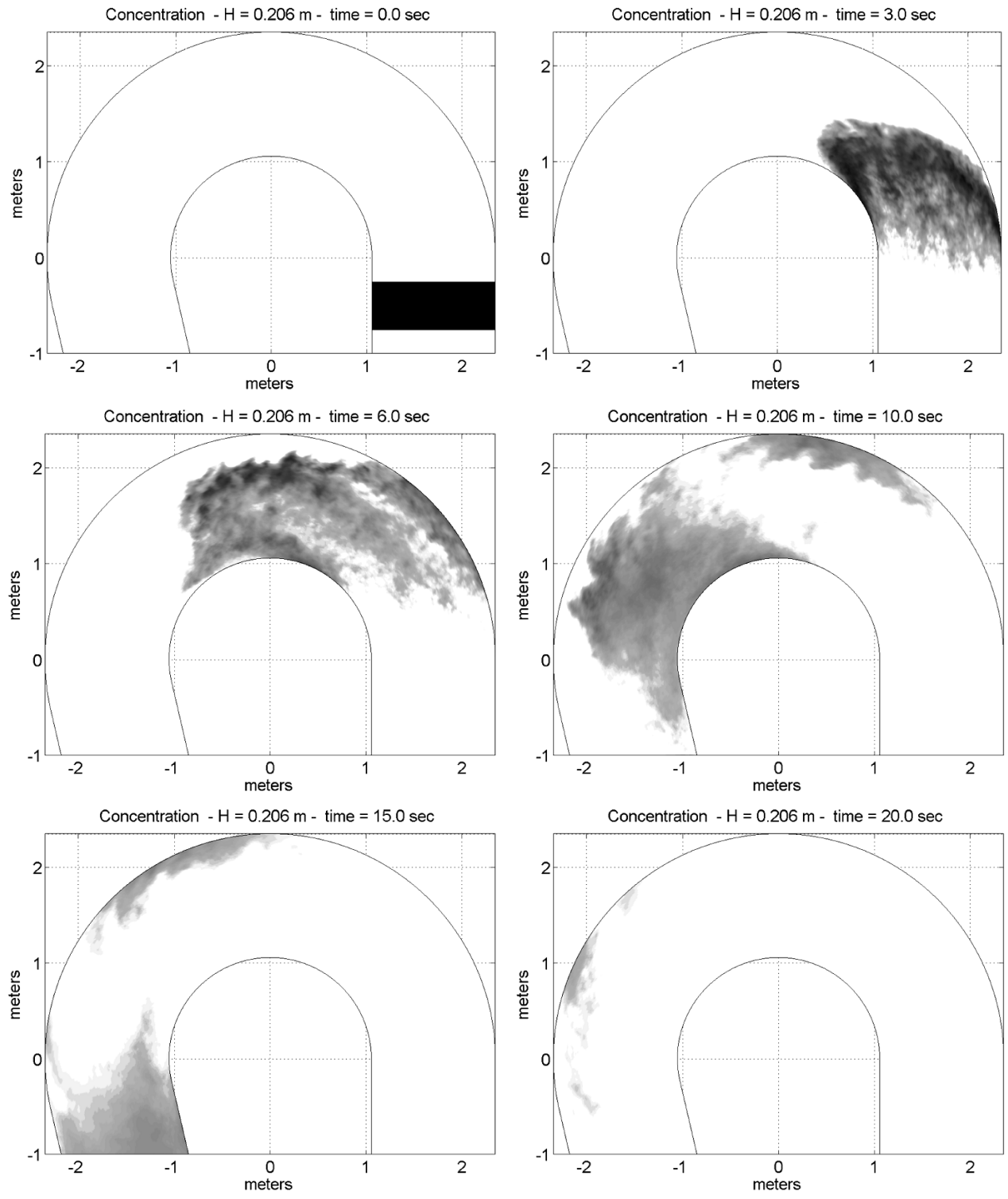

Figure 7. In lexicographic ordering: depth-averaged instantaneous concentration field at 0 s, 3 s, 6 s, 10 s, 15 s and 20 s after release.

taminant first leaves the bend near the inner bank. As the internal layer is present with great emphasis in the deep case as well as in the medium case, the rate of outflow during this stage is lower in these cases compared to the shallow case.

During stage *B.*, the bulk amount of the contaminant arrives at the exit of the bend and leaves the bend together with the amount of contaminant that was hindered in the decelerating area due to the internal shear layer. This results in a high outflow rate of the contaminant for the medium case and particularly for the deep case.

During stage *C.*, the outflow rate of the two deeper cases is lowered since during this stage the remnant amount of contaminant, previously present in the outer bank region of the bend, leaves the curved part of the flume. Because the shallow case does not suffer from the decelerating effect of the outer bank cell so strongly, the outflow rate is quite the same as during stage *B*.

After about 25 s (i.e. $\langle t \rangle > 2$), the remnant amount of contaminant is just washed out of the flume, whereafter from about 30 s the flume is entirely clean again for each case. Effectively, the residence time of the contaminant cloud is on average more or less the same for each case, whereas the transport processes are rather different.

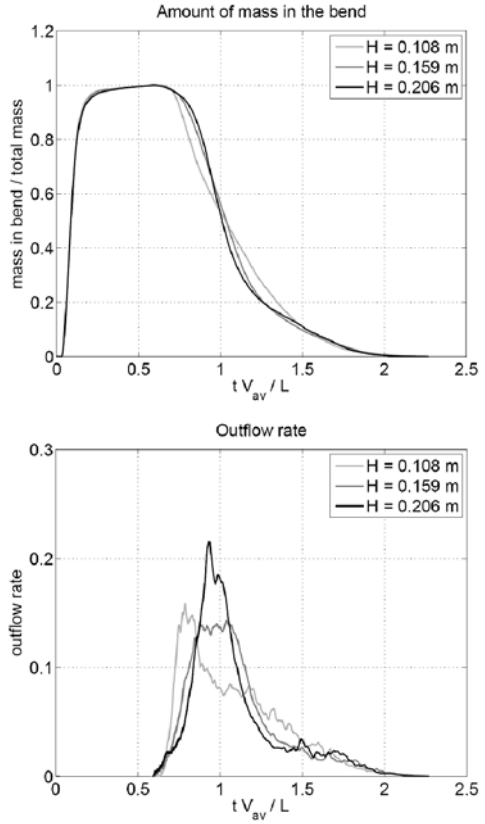

Figure 8. Amount of mass and outflow rate in the curved part of the flume normalized with the total injected amount of mass.

6 CONCLUSIONS

In this paper, we have investigated the consequences of differences in water depth for the scalar spreading in the flow through a particular flow geometry. The proper reproduction of the center region cell, the outer bank cell and internal shear layer near the inner bank turned out to be of eminent importance for the sound prediction of the scalar spreading throughout the flow. On the basis of predictions of the scalar spreading from a continuous line source and from an instantaneously injected blob it was found that the downstream inner bank region and the upstream outer bank region are regions of decelerating flow and therefore regions where the contaminant tends to accumulate. For shallow flows, it was found that these decelerating effects are very weak which makes the contaminant spread gently along the flow, whereas for deep flows it was found that these decelerating effects are very strong. Particularly the outer bank region can act like a kind of dead zone since in this area the flow is decelerating and the velocities are small. This effect becomes stronger with increasing water depth.

An analysis of the computed diffusion coefficients resulted in the observation that the gradient-diffusion hypothesis, which implies a linear dependency of the Reynolds fluxes on the mean concentration gradients, is only valid for the transport in vertical direction. For the transport in transverse direction, the linear dependency is weak, whereas it is absent in streamwise direction. Mainly in streamwise direction, counter-gradient diffusion is observed which would imply a negative diffusion coefficient. It was found that the transport in the three directions is far from isotropic. Since for these, the convection-diffusion equation for the scalar solute is directly resolve, there is obviously no influence of the hypothesis to the outcome of these simulations. The main conclusion is that care should be taken when applying the gradient-diffusion hypothesis in lower-dimensional models.

ACKNOWLEDGEMENTS

This work is supported by the Dutch Technology Foundation (STW), applied science division of NWO and the Technology Programme of the Ministry of Economic Affairs.

REFERENCES

Blanckaert K., *Flow and turbulence in sharp open-channel bends,* Ph.D. thesis, EPFL Lausanne, 2002.

Blanckaert K., Saturation of curvature induced secondary flow, energy losses and turbulence in sharp open-channel bends. Laboratory experiments, analysis and modeling, *J.Geoph.Res. 114 F03015*, 2009

Crimaldi J.P., M.B. Wiley & J.R. Koseff, The relationship between mean and instantaneous structure in turbulent passive scalar plumes, *J.Turb. 3(14)*, 2002

Demuren A.O. & W. Rodi, Calculation of flow and pollutant dispersion in meandering channels, *J.Fl.Mech. 172*, 1986

Deng Z., V.P. Singh & L.Bengtsson, Longitudinal dispersion coefficients in straights rivers, *J.Hydr.Eng. 127*, 2001

Fackrell J.E. & A.G. Robins, Concentration fluctuations and fluxes in plumes from point sources in a turbulent boundary layer, *J.Comp.Phys. 61,* 2000

Fisher H.B., The effect of bends on dispersion in streams, *Wat.Resour.Res. 5(2),* 1969

Muppidi S. & K. Mahesh, Direct numerical simulation of passive scalar transport in transverse jets*, J.Fl.Mech. 598*, 2008

Shiono K. & T.Feng, Turbulence measurements of dye concentration and effects of secondary flow on distributon in open channel flows, *J.Hydr.Eng.129*, 2001

Tagawa M., F. Matsubara & Y. Ohta, Heat transfer characteristics of a non-premixed turbulent flame formed in a curved rectangular duct, *Comb.Fl. 129*, 2002

Van Balen W., K. Blanckaert & W.S.J. Uijttewaal, Analysis of the role of turbulence in curved open-channel flow at different water depths by means of experiments, LES and RANS, *J.Turbulence, vol. 10 nr.12,* 2010.

Wagner C., S. Kuhn & P.R. von Rohr, Scalar transort from a point source in flows over wavy walls, *Exp.Fl. 43,* 2007

Wang L., Y.H. Dong & X.Y. Lu, An investigation of turbulent open channel flow with heat transfer by large eddy simulation, *Comp.Fl. 34*, 2005